AD-A164 730 ROAD DETECTION ON RADAR IMAGERY(U) MNEMONICS INC SALINE 1/1
MI J J KIM ET AL. SEP 85 ETL-0403 DACA76-84-C-0003

UNCLASSIFIED F/G 17/9 NL

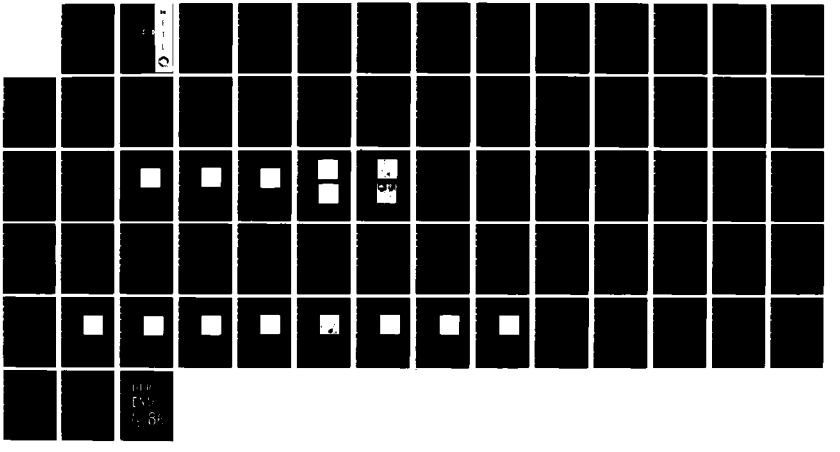

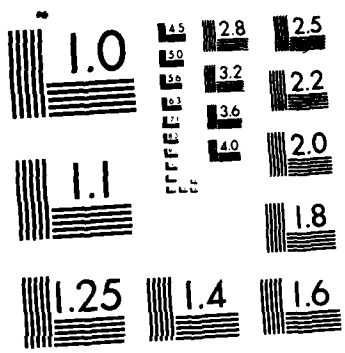

MICROCOPY RESOLUTION TEST CHART
NATIONAL BUREAU OF STANDARDS-1963-A

AD-A164 730

ETL-0403

(2)

Road detection on radar imagery

DTIC
ELECTE
FEB 27 1986
S D
D

Jungwhan J. Kim
Robert M. Haralick

Mnemonics, Inc.
Saline, Michigan 48176

September 1985

DTIC FILE COPY

APPROVED FOR PUBLIC RELEASE; DISTRIBUTION IS UNLIMITED.

Prepared for
U.S. ARMY CORPS OF ENGINEERS
ENGINEER TOPOGRAPHIC LABORATORIES
FORT BELVOIR, VIRGINIA 22060-5546

86 2 27 015

ETL

U.S. ARMY ENGINEER TOPOGRAPHIC LABORATORIES
ETL

Destroy this report when no longer needed.
Do not return it to the originator.

The findings in this report are not to be construed as an official Department of the Army position unless so designated by other authorized documents.

The citation in this report of trade names of commercially available products does not constitute official endorsement or approval of the use of such products.

UNCLASSIFIED

SECURITY CLASSIFICATION OF THIS PAGE (When Data Entered)

REPORT DOCUMENTATION PAGE		READ INSTRUCTIONS BEFORE COMPLETING FORM
1. REPORT NUMBER ETL–0403	2. GOVT ACCESSION NO. AD-A164736	3. RECIPIENT'S CATALOG NUMBER
4. TITLE (and Subtitle) ROAD DETECTION ON RADAR IMAGERY		5. TYPE OF REPORT & PERIOD COVERED Final Technical Report March 1984 - June 1985
		6. PERFORMING ORG. REPORT NUMBER
7. AUTHOR(s) Jungwhan J. Kim Robert M. Haralick		8. CONTRACT OR GRANT NUMBER(s) DACA76–84–C–0003
9. PERFORMING ORGANIZATION NAME AND ADDRESS Mnemonics, Inc. Saline, Michigan 48176		10. PROGRAM ELEMENT, PROJECT, TASK AREA & WORK UNIT NUMBERS
11. CONTROLLING OFFICE NAME AND ADDRESS U.S. Army Engineer Topographic Laboratories Fort Belvoir, Virginia 22060-5546		12. REPORT DATE September 1985
		13. NUMBER OF PAGES 62
14. MONITORING AGENCY NAME & ADDRESS(if different from Controlling Office)		15. SECURITY CLASS. (of this report) Unclassified
		15a. DECLASSIFICATION/DOWNGRADING SCHEDULE

16. DISTRIBUTION STATEMENT (of this Report)

Approved for public release; distribution is unlimited.

17. DISTRIBUTION STATEMENT (of the abstract entered in Block 20, if different from Report)

18. SUPPLEMENTARY NOTES

19. KEY WORDS (Continue on reverse side if necessary and identify by block number)

Linear features
Radar imagery
Remote sensing
Road network detection

20. ABSTRACT (Continue on reverse side if necessary and identify by block number)

Detecting a road network on radar imagery is becoming a new area in remote sensing. This report is an attempt to build a facet-based road network detection procedure for radar imagery. This procedure includes the line detection part and the road detection and connection part. The first part analytically detects linear features using a facet valley-finding technique which looks for the first directional derivative zero-crossing of a bicubic facet model. The second part statistically screens the linear features on a component-by-component base and then optimally connects the screened linear features using a dynamic programming algorithm.

DD FORM 1 JAN 73 1473 EDITION OF 1 NOV 65 IS OBSOLETE

UNCLASSIFIED

SECURITY CLASSIFICATION OF THIS PAGE (When Data Entered)

PREFACE

The work documented in this report was performed under contract DACA76–84–C–0003 for the U.S. Army Engineer Topographic Laboratories, Fort Belvoir, Virginia, by Mnemonics, Inc., Saline, Michigan. The Contracting Officer's Technical Representative was Dr. Frederick W. Rohde.

TABLE OF CONTENTS

LIST OF ILLUSTRATIONS

odes
or
A-1

CHAPTER 1 INTRODUCTION

The computer recognition of roads on remotely sensed imagery has been one of the fundamental tasks in remote sensing. Many attempts have been made on satellite images or aerial photographs but few on radar images. Our goal is to locate roads (possibly a road network) on radar imagery. The radar image differs from other remotely sensed images in that it is formed by an active system while others are formed by passive systems. As a result, it has different properties and may need somewhat different image processing techniques such as noise removal, feature detection, and segmentation. Here we propose a facet based road detection procedure for radar imagery.

In this chapter, we overview this report after the short discussion of a radar system and its characteristics.

1.1 RADAR IMAGE SYSTEM

Radar is the acronym for Radio Detection and Ranging. Radar has been developed for navigation, target detection, and reconnaissance imagery since the reflection of radio waves from solid objects was discovered. Radar imagery is acquired by a complex system. A typical radar system consists of a

transmitter, a receiver, antennas, and a recoder (see figure 1).

The transmitter emits a series of short pulses of, generally, a single wavelength through the transmitting antenna. A portion of the energy incident upon a surface is scattered back toward the receiving antenna. The receiver takes the output of the receiving antenna and amplifies its strength. The result is sequentially recorded in the recoder or displayed as a raw image for the user. To obtain a photo-like radar image, the recorded backscatters are further compiled and processed through a complicated imaging system, the study of which is beyond the scope of this report. A typical radar image is shown in figure 2.

The backscatter from the terrain to the receiving antenna is called radar return. The strong radar returns make a image brighter. The intensity of radar returns in a system is determined by the terrain properties such as complex dielectric constant and surface roughness. The effect of dielectric properties on the radar returns are usually not very strong and are therefore neglected in the radar image interpretation. The surface roughness of terrain is generally the dominent factor in determining the return intensity, which is in turn the gray-tone of the image. Surfaces of terrain can be grouped into three categories according to the pattern of the radar returns [1]:

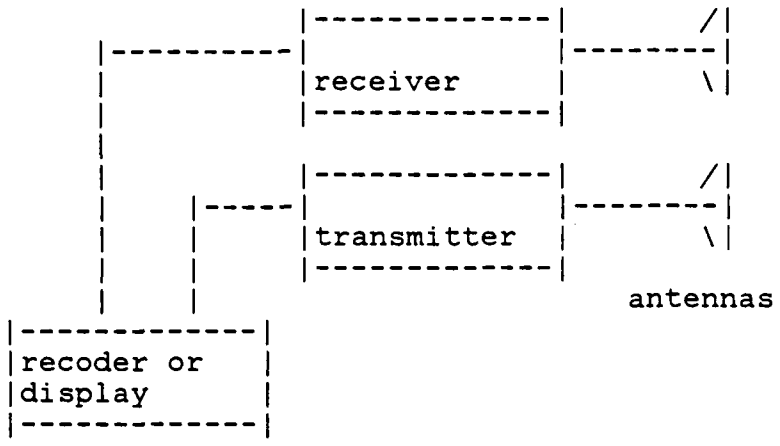

Figure 1. Structure of radar system

A smooth surface - it specularly reflects all of the incident energy in the opposite direction.

A rough surface - it diffusely scatters the incident energy in all directions.

An intermediate surface - it specularly reflects a portion of the incident energy and diffusely scatters a portion.

The classes of surfaces are closely related to radar wavelength and to the depression angle, which is defined as an angle between the horizontal line and the incident line. At a longer wavelength, the reflection of the incident energy tends to be more specular so that a resolution cell once classified at a shorter wavelength as a rough surface may

Figure 2. A typical radar image

have to be reclassified as an intermediate or smooth surface. The relationship between depression angle and surface roughness is shown in figure 3.

Rough surfaces produce almost uniformly strong returns at all depression angles. On the other hand, smooth surfaces produce little or no returns at most of the depression angles except at very high angles near vertical, where the returns are very strong. As a result, smooth surfaces such as still-water surfaces, dry lake beds, paved roads, and airport runways usually show up dark in radar images, whereas rough surfaces such as coarse gravel show up bright. In addition to rough surfaces, metalic objects and corner reflectors such as bridges and buildings also produce strong radar returns.

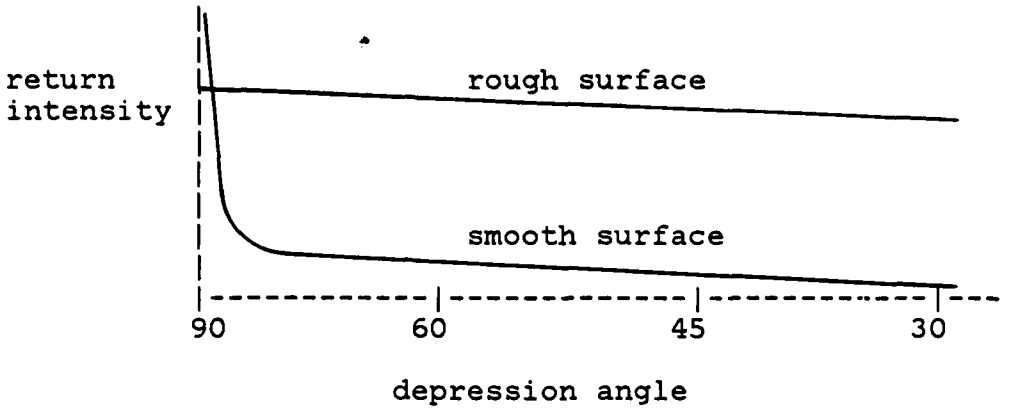

Figure 3. Return intensity: a function of surface roughness and depression angle

Other important factors influencing the appearance of radar images are shadows and highlights which are produced due to the topography of the terrain and the look direction. For example, the oblique illumination of a Side Looking Airborne Radar (SLAR) produces strong returns, called highlights, from the sides of ridges facing the antenna, and no returns, called shadows, from the other sides (see figure 4).
A radar look direction can enhance or subdue linear features on a radar image.

In this section, we overviewed a radar system and its characteristics, which would give us the insight of a road appearance in a radar image. Based on this insight and general road characteristics, our road detection project has been

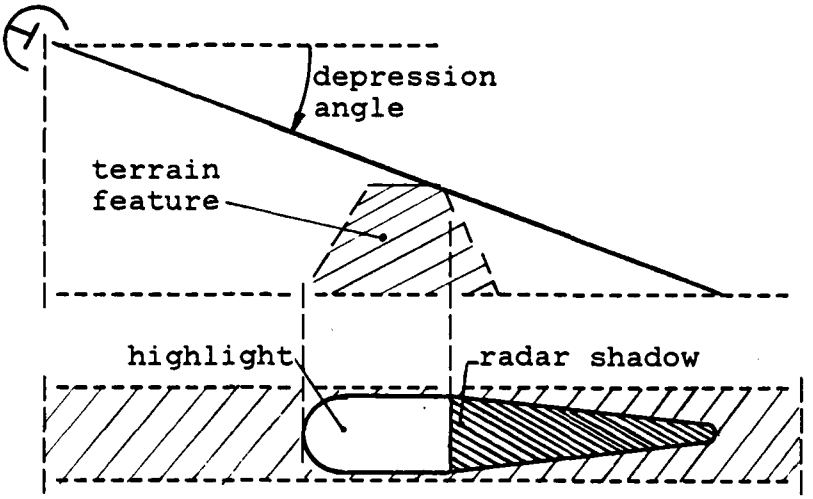

Figure 4. Highlight and shadow

started. The next section overviews the road detection procedure.

1.2 OVERVIEW

The ultimate goal of this report is to build an effective procedure which can locate road networks on radar imagery. This goal is divided into three subgoals. The first subgoal is to detect linear features on a radar image since we know roads appear as linear features in an image. The detected linear features may include non-road objects such as rivers, water passages, radar shadows, noise, and various artifacts. The second subgoal is to screen those non-road linear features. The surviving linear features, called road segments, are not usually connected to each other. The third subgoal is to connect those road segments.

The first subgoal starts with approximating a discrete digital image as continuous gray-tone intensity surface, which is expressed as a linear combination of tensor products of two set of discrete orthogonal polynomials. Using these continuous surfaces, we can obtain linear features analytically by looking for the first directional derivative zero-crossing.

For the second subgoal, the relation between the properties of roads appearing in a radar image and the statistics of the maximally connected linear features, called a component, is

analized. The properties of roads are connectivity, local straightness, contrast, etc. The statistics derived from a component are the number of pixels, average contrast, average angle difference, average gray-tone value etc. Using these properties and statistics, the road segments are differentiated from other linear features.

The third subgoal employs a dynamic programming algorithm which finds the minimum cost paths between disconnected road segments. The cost used here is evaluated for each pixel by the cost evaluation function which measures how close the statistics of a pixel are to those of an assumed real road pixel.

Chapters 2 and 3 deal with the road detection procedure, which is the main body of the report. Especially chapter 3 elaborates the principle and application of the dynamic programming in image processing. Finally, chapter 4 shows the experimental results on a few SAR (Synthetic Aperture Radar) images.

CHAPTER 2 LINE DETECTION

2.1 INTRODUCTION

To detect linear features we use the modified version of the ridge-valley algorithm originally suggested by Haralick [2]. In this chapter, the algorithm is discussed from the view point of road detection on a radar image. The road on a radar image usually appears as a dark line which can be loosely defined as a connected sequence of pixels having significantly lower gray-tone intensity than the neighbors. In a continous gray-tone surface, the dark line would be viewed as a valley which could be computed analytically; the bottom of a valley would occur where the first directional derivative of the surface has a zero-crossing and the second derivative is positive. Such a surface can be obtained from a discrete image by a facet model generating function which is discussed in section 1. Then, a facet based line detection algorithm is discussed in section 2.

2.2 FACET MODEL

The idea of using a fitted continous model in image processing has been proposed [3]. A fitted model for image data is

called a facet model. A facet model can be produced by a facet generating function K;

$$K : D(I) \times O \times \{B\} \times \{I\} \rightarrow f^*(R) \qquad (4.2.1)$$

The D(I) is discretely sampled data function, that is a digital picture. The O is the order of fit. For example, when using the second order of fit, the resulting facet model will be a quadratic polynomial. The index set {I} is the domain on which the discretely sampled data function D(I) and a set of basis functions {B} are defined. The {B} is a set of discrete orthogonal functions. The $f^*(R)$, a real valued function, is called a facet model. Here, we discuss how the function K maps arguments into a facet model when {B} is a set of discrete Chevyshev polynomials, O, the third order of fit, and {I}, a two-dimensional integer index set {(r,c)} where $-n \leq r \leq n$ and $-m \leq c \leq m$. Since it is the third order fit and {I} is a two-dimensional index set, it is assumed that the continous gray-tone intensity surface f, from which D(I) is discretely sampled, takes the parametric form of a bicubic polynomial defined in the row-column coordinates. Generally, the function f is expressed by

$$f(r,c) = k_1 + k_2 r + k_3 c + k_4 r^2 + k_5 rc + k_6 c^2 + k_7 r^3 + k_8 r^2 c + k_9 r c^2 + k_{10} c^3 \qquad (4.2.2)$$

The value f^* of function K is then obtained by estimating the coefficients of Eq. (2.2.2). The least square error method directly applied to Eq. (2.2.2) can give the solution to the problem of estimating the coefficients. However, the computation is very complex. An alternative is that after expressing the function f as another form, a linear combination of discrete orthogonal polynomials {B}, the new form of the function f is used in the same method. Let {B} be $\{R_0, \ldots, R_n\}$. Then, the function f is expressed by

$$f(r,c) = \sum_{n=0}^{N-1} b_n R_n(r,c) \qquad (4.2.3)$$

By least square error method, the coefficients $b_0, \ldots, b_n$ of Eq. (2.2.2) are estimated instead of the coefficients $k_1, \ldots, k_{10}$ of Eq. (2.2.2). By doing so, we can use the orthogonality of the basis functions {B}, and hence achieve much less complex computation.

The discrete Chevyshev polynomials defined on the integer index set {(r,c)} are constructed inductively in the following way. Let P_n be the nth order polynomial. Define $P_0 = 1$ and suppose $P_1(r), \ldots, P_{n-1}(r)$ have been constructed. Then $P_n(r)$ must be orthogonal to each polynomial $P_0(r), \ldots, P_{n-1}(r)$. That is,

$$\sum_{r} P_k(r)\, P_n(r) = 0, \text{ for all } k \le n-1 \qquad (4.2.4)$$

where $P_n(r) = r^n + a_{n-1}r^{n-1} + \ldots + a_1 r + a_0$. Solving the unknowns $a_0, \ldots, a_{n-1}$ from the n linear equations, we construct $P_n(r)$. The set $\{P_0(r), \ldots, P_n(r)\}$ is a one-dimensional discrete orthogonal polynomial set for the integer index set $\{r\}$. A two-dimensional discrete orthogonal polynomial set for the integer index set $\{(r,c)\}$ can be easily constructed by taking the tensor products of two one-dimensional sets, $\{P_0(r), \ldots, P_n(r)\}$ and $\{Q_0(c), \ldots, Q_n(c)\}$. For example, on the two-dimensional index set $\{-1, 0, 1\} \times \{-1, 0, 1\}$, the discrete Chevyshev polynomial set can be defined as the tensor products of $\{1, r, r^2 - 2/3\}$ and $\{1, c, c^2 - 2/3\}$, which yields $\{1, r, c, r^2 - 2/3, rc, c^2 - 2/3, r(c^2 - 2/3), c(r^2 - 2/3), (r^2 - 2/3)(c^2 - 2/3)\}$.

Now we go back to the problem of estimating the coefficients of Eq. (2.2.3). Let D(r,c) be the discretely observed data function. Then, the square error is expressed by

$$e^2 = \sum_{(r,c)} \left[D(r,c) - \sum_{n=0}^{N-1} b_n R_n(r,c)\right]^2 \qquad (4.2.5)$$

The coefficient, b_i of the ith order discrete orthogonal polynomial $R_i(r,c)$ can be computed by the partial derivative of e^2 with respect to b_i.

$$\frac{\partial e^2}{\partial b_i} = -2 \sum_{(r,c)} \left[D(r,c) - \sum_{n=0}^{N-1} b_n R_n(r,c) \right] [R_i(r,c)] \quad (4.2.6)$$

Using the orthogonality of the polynomials $R_0(r,c)$, ..., $R_{N-1}(r,c)$, we know

$$\sum_{(r,c)} [R_j(r,c)\, R_i(r,c)] = 0, \text{ for all } j \neq i \quad (4.2.7)$$

Thus the Eq. (2.2.6) is reduced to

$$\frac{\partial e^2}{\partial b_i} = 2 b_i \sum_{(r,c)} [R_i(r,c)]^2 - 2 \sum_{(r,c)} [D(r,c)\, R_i(r,c)] \quad (4.2.8)$$

Setting the partial derivative of e^2 with respect to b_i to zero we obtain the estimate b_i^* of the coefficient b_i.

$$b_i^* = \sum_{(r,c)} [D(r,c)\, R_i(r,c)] / \sum_{(r,c)} [R_i(r,c)]^2 \quad (4.2.9)$$

It should be noted that each coefficient b_i ($i \leq N-1$) is just a linear combination of the data values $D(r,c)$. In other words, b_i^* is simply obtained by multiplying the data value $D(r,c)$ by the weight

$$R_i(r,c) / \sum_{(r,c)} [R_i(r,c)]^2 \quad (4.2.10)$$

for each index (r,c). Once the coefficient b_i ($i \leq N-1$) have been computed, the estimate f^* of the continous function f is given by

$$f^*(r,c) = \sum_{n=0}^{N-1} b_n^* R_n(r,c) \qquad (4.2.11)$$

Eq.(2.2.11) gives the estimates of the coefficients k_1, ..., k_{10} of the bicubic polynomial Eq. (2.2.2).

In this section, we discussed one instance of facet models which can be generated by the facet generating function K. It is notable that various facet models can be generated by changing arguments in the function K. Image processing techniques based on a facet model have been developed. Among them are the directional derivative edge detector [4] and the ridge-valley finder [2]. In the next section we will see a line detection algorithm based on a bicubic facet model, which is the modified version of the ridge-valley finder, and is used for the detection of lines having a constant width.

2.3 ALGORITHM

The canonical form of the fitted bicubic surface for each pixel's neighborhood of an input image is

$$f(r,c) = k_1 + k_2 r + k_3 c + k_4 r^2 + k_5 rc + k_6 c^2$$

$$+ k_7 r^3 + k_8 r^2 c + k_9 r c^2 + k_{10} c^3 \qquad (4.3.12)$$

The first directional derivative of a function f in the direction α, f'_α is defined by

$$\begin{aligned} f'_\alpha(r,c) &= \lim_{d \to 0} \frac{f(r + d\sin\alpha,\ c + d\cos\alpha) - f(r,c)}{d} \\ &= \frac{\partial f}{\partial r}(r,c)\sin\alpha + \frac{\partial f}{\partial c}(r,c)\cos\alpha \end{aligned} \qquad (4.3.13)$$

Similarly, the second directional derivative of f is defined by

$$\begin{aligned} f''_\alpha(r,c) = {} & \frac{\partial^2 f}{\partial r^2}(r,c)\sin^2\alpha + 2\frac{\partial^2 f}{\partial r \partial c}(r,c)\sin\alpha\cos\alpha \\ & + \frac{\partial^2 f}{\partial c^2}(r,c)\cos^2\alpha \end{aligned} \qquad (4.3.14)$$

The direction α for which f''_α is an extremum can be determined by setting the derivative of f''_α with respect to α to zero.

$$\frac{\partial f''_\alpha}{\partial \alpha} = \left(\frac{\partial^2 f}{\partial r^2} - \frac{\partial^2 f}{\partial c^2} \right) \sin 2\alpha + 2\frac{\partial^2 f}{\partial r \partial c}\cos 2\alpha \qquad (4.3.15)$$

Solving Eq. (2.3.15) we obtain

$$\begin{aligned} \sin 2\alpha &= \pm (-2\partial^2 f/\partial r \partial c)/D \quad \text{and} \\ \cos 2\alpha &= \pm (\partial^2 f/\partial r^2 - \partial^2 f/\partial c^2)/d \end{aligned} \qquad (4.3.16)$$

where

$$D = [\ 4\ (\partial^2 f/\partial r \partial c)^2 + (\partial^2 f/\partial r^2 - \partial^2 f/\partial c^2)^2\ ]^{0.5}$$

Substituting Eq. (2.3.12) into Eq. (2.3.16), we can get the direction α at the center of each pixel, which is the direction normal to an assumed valley line through the pixel.

$$\alpha = \pm\ 0.5\ \tan^{-1}\ k_5/(k_6 - k_4) \qquad (4.3.17)$$

Using the angle α to constrain a position (r, c), we know

$$r = \rho\ \sin\alpha \quad \text{and} \quad c = \rho\ \cos\alpha$$

Thus, the cross-section of the surface in the direction α through the origin is given by

$$f_\alpha(\rho) = A\rho^3 + B\rho^2 + C\rho + k_1 \qquad (4.3.18)$$

where

$$A = k_7\ \sin^3\alpha + k_8\ \sin^2\alpha\ \cos\alpha + k_9\ \cos^2\alpha\ \sin\alpha + k_{10}\ \cos^3\alpha,$$
$$B = k_4\ \sin^2\alpha + K_5\ \sin\alpha\ \cos\alpha + k_6\ \cos^2\alpha, \text{ and}$$
$$C = k_2\ \sin\alpha + k_3\ \cos\alpha. \qquad (4.3.19)$$

The typical curve of Eq. (2.3.18) is shown in figure 5.

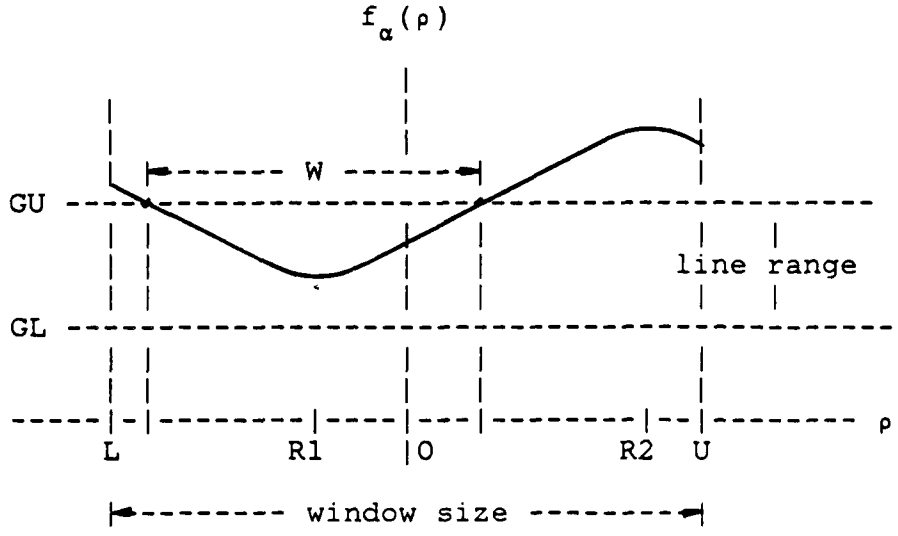

Figure 5. Cross section of surface

In the figure R1 and R2 are the zero-crossings of Eq. (2.3.18) and L and U are the lower and upper limit of domain which is determined by a window size. Assume that R1 is closer to the center of pixel than R2. Then we can declare the pixel as a line pixel if all of the following conditions are satisfied:

1. The first derivative of Eq. (2.3.18) has a zero-crossing sufficiently near the pixel's center and the second derivative is positive at the zero-crossing point;

$$|R1| < \text{threshold}_1 \quad \text{and} \quad \frac{d^2 f_\alpha(R1)}{d\rho^2} > 0 \qquad (4.3.20)$$

2. The curvature of the curve is big enough;

$$\left| \frac{d^2 f_\alpha(0)}{d\rho^2} \right| > \text{threshold}_2 \qquad (4.3.21)$$

3. The gray-tone of the pixel is within a proper line range;

$$\text{threshold}_3 \le f_\alpha(R1) \le \text{threshold}_4 \qquad (4.3.22)$$

4. The contrast of the pixel with its surrounding is sufficiently large;

$$\text{MIN}\,[f_\alpha(L),\ f_\alpha(R2)] - f_\alpha(R1) > \text{threshold}_5 \qquad (4.3.23)$$

(The thresholds are provided by the user)

Once a line pixel is identified, it is assigned four property values which are shown in figure 11 and defined as follows:

1. Depth, $D = f_\alpha(R1)$
2. Strength, $S = \text{MIN}\,[f_\alpha(L),\ f_\alpha(R2)] - f_\alpha(R1)$
3. Angle, $A = \alpha$
4. Width, W = the number of pixels whose gray-tone values are in the line range.

These property values can be utilized in further processing. For example, by setting W to 2 we can detect two pixel wide lines and then by restricting A we can find two pixel wide lines at a certain orientation.

In this section we discussed the line pixel detection algorithm on a pixel by pixel base. That is, based on the bicubic facet model for each pixel, we looked for a zero-crossing point which satisfies a set of constraints. If such a point was found within its neighborhood we declared the pixel as a line pixel.

2.4 EXPERIMENTS

The line detection algorithm was tested on a few SAR images. The results are dependent on the combination of the thresholds. Figure 6 through figure 8 show the effects of the thresholds for which a 100 x 100 subimage shown in figure 23 was used as a test image.

The $threshold_1$ is called radius. Figure 6 shows how the radius affects the results. It is noted that a bigger radius value gives thicker lines. For our purpose, a radius between 1.2 and 1.5 turned out to be the most effective.

The threshold$_2$, called curvature, has the effect of eliminating the artifacts but also has a tendency to break a line into shorter pieces, as shown in figure 7. A curvature around 750 was best for the image with a gray-tone scale of 0 through 65,535.

The threshold$_3$ and threshold$_4$ give the gray-tone bounds within which line pixels should lie. Using these thresholds we obtain lines in our intended gray-tone range. They have the same effect as the intensity line operator described in Fischler et al [5]. Their effects on the result are shown in figure 8.

Threshold$_5$, called contrast, reflects the human visual recognition of lines. That is, a vivid line in a bright area may not be as perceptible as it is in a darker area. As a result, the higher contrast threshold gets rid of relatively vague lines and tends to loose useful information. For our next process which requires a lot of information, this threshold had to be lowered.

The total results of the line detection technique are shown in figures 9 and 10.

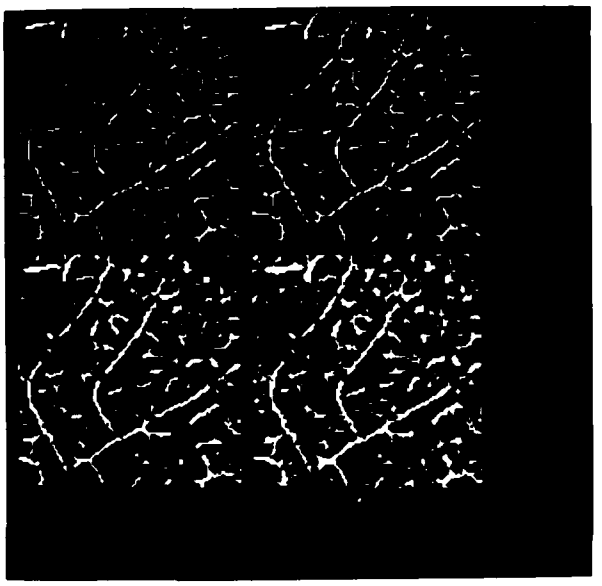

Figure 6. The effect of radius: Upper left (radius = 0.75), Upper right (radius = 1.00), Lower left (radius = 1.50), Lower right (radius = 2.00)

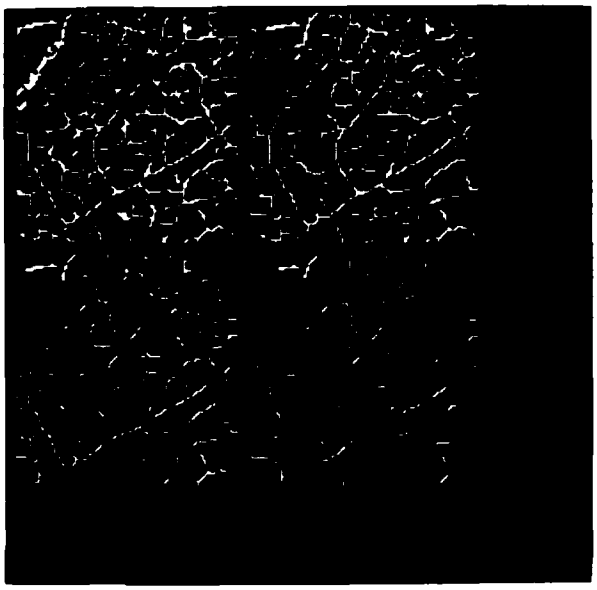

Figure 7. The effect of curvature: Upper left (curvature = 100), Upper right (curvature = 500), Lower left (curvature = 750), Lower right (curvature = 1000)

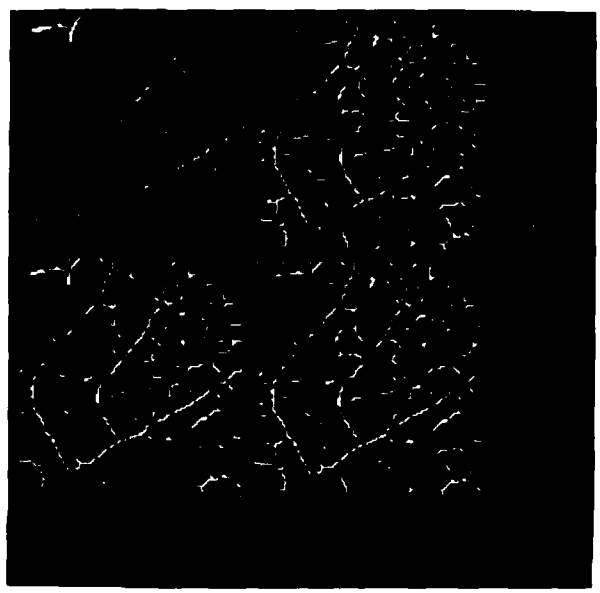

Figure 8. The effect of gray-tone range: Upper left (equiv. range = 1000 -- 2000), Upper right (equiv. range = 2000 -- 3000), Lower left (equiv. range = 1500 -- 2500), Lower right (equiv. range = 1800 -- 2700)

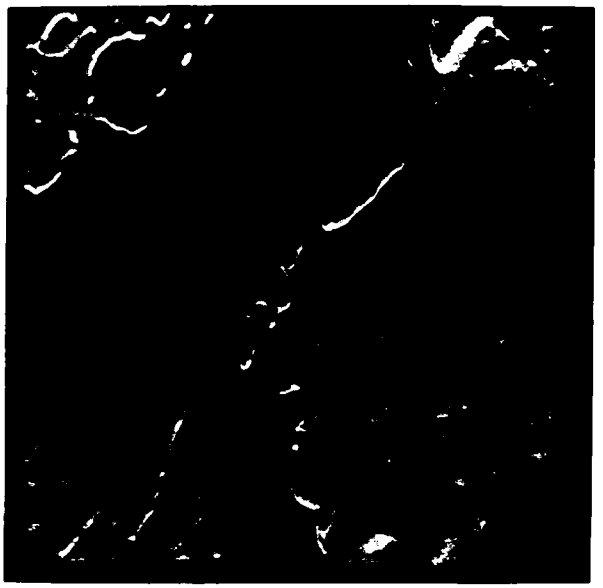

a. Original image

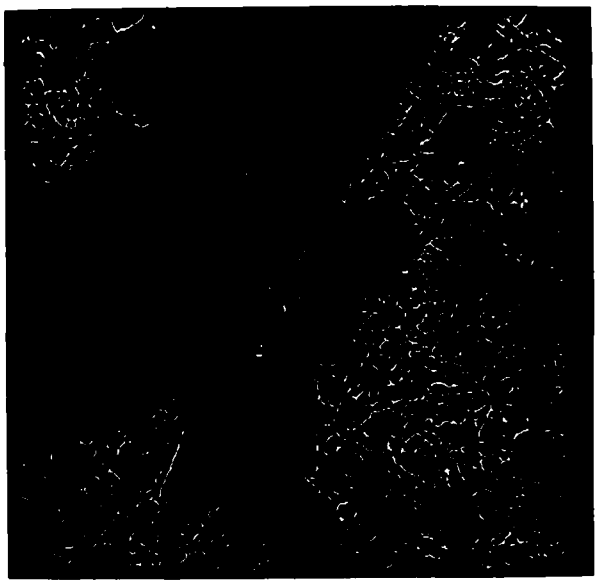

b. Line image

Figure 9. Huntsville area: Curvature = 750, Radius = 1.2, Equiv. range = 1500 thru 3000, Contrast = 800, Width = 1 thru 4

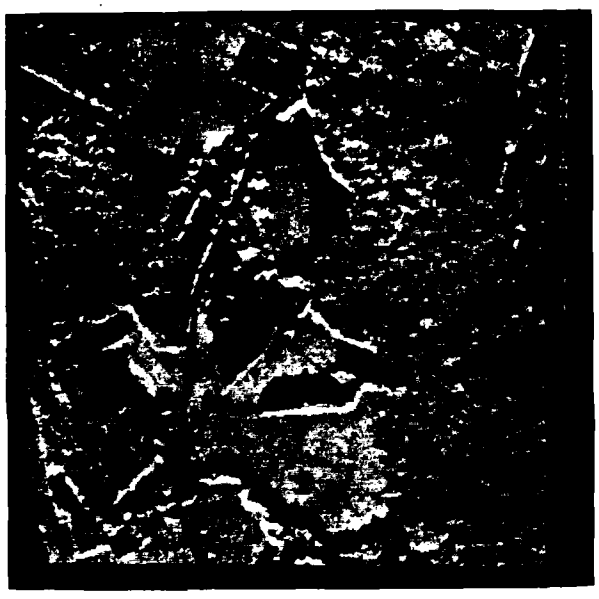

a. Original image

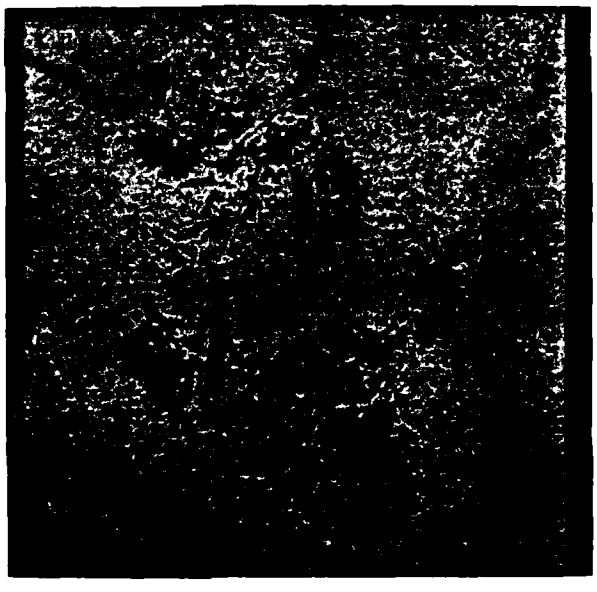

b. Line image

Figure 10. Elizabeth city area: Curvature = 750, Radius = 1.4, Equiv. range = 1800 thru 2700, Contrast = 1000, Width = 1 thru 4

CHAPTER 3 ROAD DETECTION AND CONNECTION

3.1 INTRODUCTION

The line detector discussed in the previous chapter gives plenty of information about a line pixel such as strength, gray-tone value, angle, and width. However, the information provided by the detector includes many non-road linear objects. At the beginning of our research, these non-road linear objects seemed to be easy to remove by adjusting the thresholds of the line detector. This resulted in the waste of time in search of a proper combination of the thresholds. But we soon learned and developed the idea of screening the linear features on a connected component by connected component base, not on a pixel by pixel base. This screening technique uses the statistics of each connected component. To get the neccessary statistics efficiently, the line pixels are connected first, using 8-connectivity. Each maximally connected set of pixels is called a component. Each component is then assigned an integer identifier. The statistics can be derived from each component. The details are discussed in section 2.

Other important factors in the screening process are the road characteristics appearing in radar imagery. Those characteristics are:

1. The road should be connected.
2. The road should be a linear feature.
3. The road should be sufficiently straight or smoothly curved.
4. The road should be contrasted with its surroundings.
5. The road should have a sufficiently low gray-tone intensity.

On the basis of these road characteristics in conjunction with the statistics, the components are screened.

3.2 ROAD DETECTION

The road detection is closely related to the road connection which will be discussed in the next section.

If the road connection procedure did not exist and our system ended with road segments detected from the linear features, the road detection part would have been greatly different. Figure 11 illustrates the difference through the example of a very simple road network (figure 11a). Figure 11b shows the linear features detected from figure 11a. In the system without a connection procedure, the road detector would be

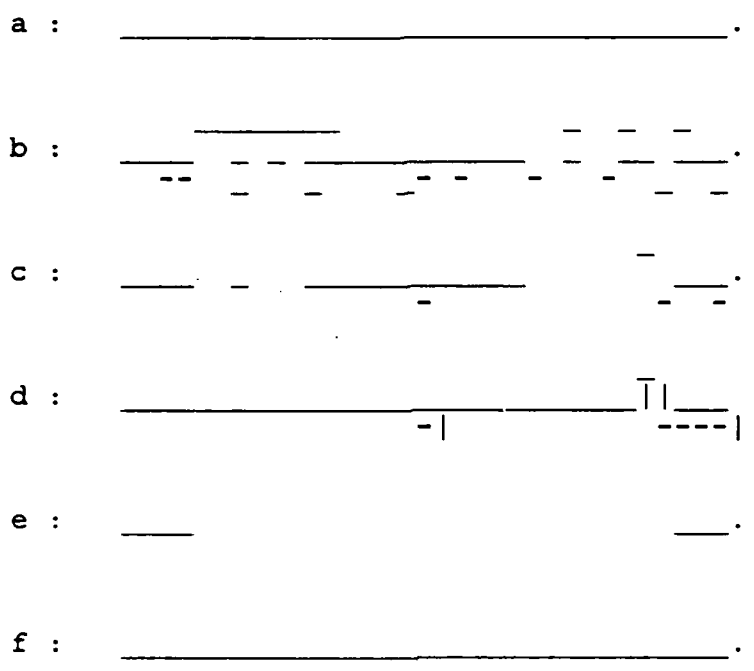

Figure 11. Detection and connection

designed to detect as many road segment as possible even though the result may include a few non-road linear features (see figure 11c). In the system with a connection part, however, the result shown in figure 11c is not very desirable because the connection procedure will connect all segments including falsely marked road segments, which yields a different network (figure 11d). To make it worse, it would take a longer processing time than the result with fewer segments because the connection procedure would be invoked more frequently. The most desirable result of the road detection in the system with a connection part is shown in figure 11e,

which requires only one invocation of the connection procedure to reconstruct the original network (figure 11f). Therefore, the road detection in the system with a connection procedure should give the smallest number of road segments that can reconstruct the original network. The road detection used in this report can be viewed as a thresholding procedure with a simple combining mechanism. This procedure uses the statistics to threshold the components, and then combines any pair of surviving components which are one pixel apart, to reduce the number of road segments. These statistics are derived from each component. Those are the number of pixels in the component (N), the mean line strength (MS), the standard deviation of line strengths (DS), the mean angle difference (MB), the mean gray-tone value (MG), and the standard deviation of gray-tones (DG). These statistics are totally dependent on the set of thresholds used in the previous line detection. The road detection is based on the relation between these statistics and road characteristics appearing in radar imagery. The intuitive meaning of each statistic is discussed next.

(1) The number of line pixels in a component (N): This value is important for identifying the real road segment. A road network is completely connected and the things that break the network into pieces are the noise in the image and the possible error in our bicubic surface. In any noisy area in a

image, unless the area is completely damaged by the noise, a road segment would have at least a certain number of connected pixels. Under the assumption that the N value of a non-road component is relatively small, a component with a sufficiently large N is considered as a road segment. The threshold against N should not be too small nor too large because too small a threshold would mistake non-road components as road segments and too large a threshold would fail to pick up road segments. An appropriate value of the threshold against N may vary image to image. In our experiments the most effective value is between 8 and 12.

(2) The mean line strength of a component (MS): The MS value indicates the contrast of a component with its neighboring region running parallel to the component. The contrast of a component for a likely road segment is assumed higher than that of a non-road component. This assumption is not always true and so the real road components are thrown away as well as non-road components when thresholing against this parameter. However, in many cases, giving up a few real road segments can get rid of many non-road components. The line pixels in the abandoned road segments are re-used for connecting the road segments later in the road connection part.

(3) The standard deviation of line strengths (DS): The line strength (contrast) of each pixel in a component for a likely

road segment is more uniform than that in a noisy component because the gray-tone intensity of a radar image is locally homogeneous. Hence, the smaller DS value has a component the more likely the component is a road segment especially when the component is not too large to lie on two or more different regions.

(4) The mean angle difference in a component (MB): The MB value is a good measurement of the staightness of a component. The angle difference of a line pixel is defined in a component as a difference in angles between adjacent pixels with the same label as itself. Since a line pixel usually has more than one adjacent pixel with the same label, the priority of the adjacent pixels are set up in a way that the angle difference of two adjacent pixels may not be used twice if possible. The priority set-up used in our experiment is shown in figure 12.

The pixel with the highest priority (the lowest number) is chosen as the adjacent pixel of center pixel X if the pixel and the center pixel are in the same component. Ideally, a perfect circle composed of 36 pixels may have 10° MA and a straight line has 0° MA. In reality, the MA value does not reflect the true situation accurately. The inaccuracy is mainly due to the error involved in the discrete data. In our experiments, components with MA values less than 15° were considered as candidates to be real road segments.

7	4	8
3	X	1
6	2	5

Figure 12. The priorities of the eight adjacent pixels

(5) The mean gray-tone value of a component (MG): This value is another important tool for differentiating a component for a possible road segment from a non-road component. Even if a component has a relatively high MS value without a sufficient darkness, the component cannot be a real road segment. It is because the surface roughness of a road segment does not vary enough to change the gray-tone, place to place, in the same image. The MG value of a road component should be in a certain range of gray-tone. Although this range is dependent upon an image brightness it is usually in between 22,000 and 28,000 in a gray-tone scale of 0 to 65,535 for the collection of radar images in our library.

(6) The standard deviation of gray-tone values (DG): This is a suplementary tool to the mean gray-tone. The gray-tone values of a non-road component is assumed to have a greater standard deviation than those of a component for a likely road segment. Re-thresholding the components against the DG values can keep the surviving non-road components from being mistaken as road components.

3.3 ROAD CONNECTION

To complete the road networks all the detected road segments are connected using the non-road pixels, whether they are line pixels or not. Among many possible connecting paths between two road segments, the path with the maximum likelihood (or the minimum cost) is chosen by a dynamic programming method. To do so all non-road pixels are evaluated by a cost evaluation function. The technique of dynamic programming and the strategy of cost evaluation function are the main subject of this section.

3.3.1 DYNAMIC PROGRAMMING

Dynamic programming is a very useful approach to optimization. It is based on the "principle of optimality"; any subpolicy of an optimum policy must be optimum itself [6]. The optimality principle is applied to finding the minimum cost path between two road segments. Similarly it holds that any subpath of the optimum (or the minimum cost) path from one (starting) segment to another (goal) segment must be optimum. The relationship of the subpath to the whole path can be defined recursively. The technique for solving an optimum path is generally described and then a tailer-made algorithm for our purpose is presented.

As shown in the figure 13, the minimum cost path from S to T is sought. Let X_i (i =°1, 2, ..., n) be a set of pixels, one of which must be part of a possible minimum cost path from S to T.

Let g(a,b) be the function which gives the minimum cost from a to b. Now suppose that the minimum cost path between S and T contains X_k. Then, the minimum cost from S to T is given by

$$g(S,T) = g(S, X_k) + g(X_k, T) \qquad (5.3.24)$$

In general, the k of X_k is unknown in advance and the minimum cost is rewritten by

$$g(S,T) = \underset{i}{MIN} [\ g(S, X_i) + g(X_i, T)\ ] \qquad (5.3.25)$$

Let's consider the special case where X_i's are the eight neighbors of the goal T and $g(X_i, T)$ is the constant, CT for all X_i's, which is the cost of advancing from each of the X_i's to T (see figure 14)

Then, the minimum cost from S to T can be expressed by

$$g(S, T) = \underset{i}{MIN}\ g(S, X_i) + CT \qquad (5.3.26)$$

Similarly each of $g(S, X_i)$'s is reduced to

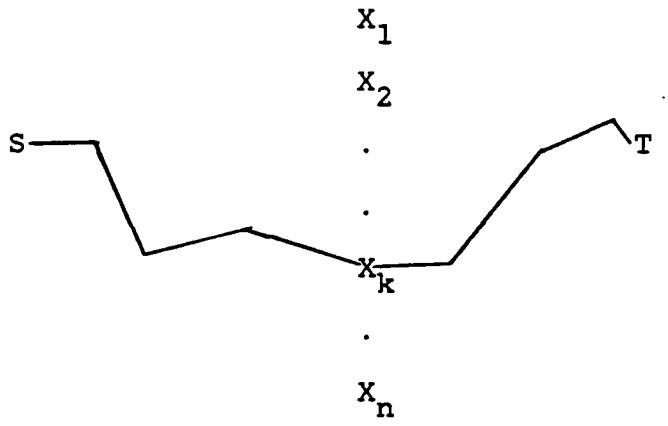

Figure 13. The minimum paths between S and X_i and T

$$g(S, X_i) = \underset{j}{\text{MIN}}\, g(S, Y_j) + CX_i \qquad (5.3.27)$$

where Y_j ($j = 1, 2, \ldots, 8$) are the eight neighbors of X_i and CX_i is the cost of advancing from the Y_j's to X_i. Accordingly we obtain the minimum cost from S to T by

$$g(S, T) = \underset{i}{\text{MIN}} \left(\underset{j}{\text{MIN}}\, g(S, Y_j) + CX_i \right) + CT \qquad (5.3.28)$$

This procedure is repeated recursively until we get

$$g(S, T) = \underset{i}{\text{MIN}} \left(\underset{j}{\text{MIN}} \left(\ldots \underset{n}{\text{MIN}}\, g(S, Z_n) + \ldots \right. \right. \\ \left. \left. \ldots \right) + CX_i \right) + CT \qquad (5.3.29)$$

where Z_n's are the eight neighbors of the starting pixel, S and $g(S, Z_n)$'s are the known values, CZ_n's, the costs of advancing from S to Z_n's.

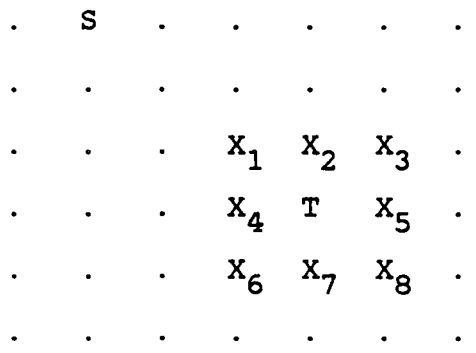

Figure 14. The special arrangement of S, X_i, and T

This basic idea has been implementated in many application areas since it was presented by Ford [7]. The F^* algorithm used in Fischler et al. [5] is an implementation nicely fitted to the sequential image processing. It is noted that the similar optimization method (e.g. the A^* algorithm in Duda and Hart [8]) can be derived from the best first search algorithm. Our implementation can be thought as a extended version of the F^*, called F^o. In our experiments, the F^o algorithm is applied iteratively in the manner of minimum cost spanning tree. Each road segment (a set of pixels) plays the role of a vertex in a graph. Each result of the F^o algorithm applied to each pair of segments plays the role of a weighted edge between vertices. Our implementation details are presented here. The prerequisite is a cost image on which the algorithm is exercised. The cost image is computed by a cost evaluation function which will be discussed in the next section. For the time being, the algorithm is assumed

to have it. The sets of starting pixels and goal pixels are specified by the real road segment image in which every road segment has a unique label. Consider the following procedure;

While the number of road segments is greater than 1

1. Set a segment to the starting segment.
2. Set the others to the goal segments.
3. Find the minimum cost path.
4. Assign the same label to the connected segments.

Each iteration of this procedure involves top-to-bottom (and bottom-to-top) passes on the cost image, C, and updates the total cost from the starting segment to each pixel, S(i,j) according to the left-to-right rule, Eq. (3.3.30), and right-to-left rule, Eq. (3.3.31);

$$\begin{aligned} S(i,j) = \text{MIN} [\ & S(i-1, j-1) + C(i, j), \\ & S(i-1, j) + C(i, j), \\ & S(i-1, J+1) + C(i, j), \\ & S(i, j-1) + C(i, j), \\ & S(i,j)] \end{aligned} \tag{5.3.30}$$

$$S(i, j) = \text{MIN} [\ S(i, j+1) + C(i, j), S(i, j)\ ] \tag{5.3.31}$$

All the costs in each row are updated from left to right and then from right to left using both of the rules. It usually needs more than one pass until it stops fo. the next iteration of the procedure. The terminating condition of the algorithm is that further passes can not update the total cost image S(i, j). The following example shows the operation of the minimum cost path finding algorithm from two sets of source pixels (subscripted by s1 or s2) to two sets of goal pixels (subscripted by g3 or g4). In the global sense, this example can be viewed as the first step of the minimum cost spanning tree through the four vertices (segments subscripted by s1, s2, g3, or g4) with two designated starting vertices (segments subscripted by s1 and s2). The cost image C(i, j) is shown in figure 15. The total cost image S(i, j) after each pass is shown in figure 16 thru figure 18. As shown in figure 17 and figure 18, there is no updates at the third pass. Accordingly the algorithm is terminated right after the third pass. The minimum cost path (the first edge to span) is found between segments subscripted s1 and g3, and its elements are bracketed in figure 18. Those segments including the path between them become a new segment for the next iteration (spanning). It should be noted that the algorithm can be terminated even after the second pass. It is because the smallest of the updated values, 5 is greater than the minimum cost, 4 after the second pass (see the asterisked

values in figure 17). In our experiments, both of the terminating conditions were implementated.

3.3.2 COST EVALUATION FUNCTION

The cost of a pixel is defined as the expense for advancing to the pixel from any of its eight neighbors. The basic strategies of cost evaluation are:

(1) A non-line pixel is penalized enough not to be chosen as a part of road network since a network can be constructed only with line pixels
(2) A line pixel is rewarded according to its attributes which are the strength (S), angle difference (B), and gray-tone distance (D).

The strength of a line pixel (S) is defined as the difference in the values of the stationary points just as defined in the earlier chapter. The definition of the angle difference of a line pixel (B) is slightly different from that of angle difference in a component which was discussed in the previous section. The angle difference of a line pixel is defined as follows. First, two neighbors are selected such that they best coincide with the angle of a pixel. Next, two differences of angles are taken; between the angle of the pixel and that of a neighbor, and between the angle of pixel and that

2	5	6	3	0_{s1}	2	1	0_{s2}
3	1	1	5	2	0_{s1}	1	7
1	3	3	3	1	6	7	5
3	4	2	7	2	5	6	4
2	1	1	1	2	1	2	1
3	1	0_{g3}	0_{g3}	2	4	3	2
4	3	5	7	0_{g3}	2	5	7
2	0_{g4}	1	1	3	2	2	1

Figure 15. A sample cost image, C(i, j)

of the other neighbor. The larger difference of the two is then the angle difference of a line pixel. Suppose that the zero angle direction is set to the positive column direction and the angles increase clockwise as shown in figure 19, and that the line pixel 5 has an angle closer to 45° than to 90°. Then, the two neighbors of pixel 5 become pixel 1 and pixel 9 and the angle difference of pixel 5 is given by

$$B = \text{MAX}\,[\text{abs}\,(\text{angle of pixel 5} - \text{angle of pixel 1}),\ \text{abs}\,(\text{angle of pixel 5} - \text{angle of pixel 9})] \qquad (5.3.32)$$

The gray-tone distance of a line pixel (D) is defined as the absolute difference in the gray-tone value of the pixel and an assumed mean gray-tone value of real road segments which

16	14	9	3	0_{s1}	2	1	0_{s2}
8	5	4	5	2	0_{s1}	1	7
6	7	7	4	1	6	7	6
9	10	6	8	3	6	12	10
8	6	5	4	5	4	6	7
8	5	4_{g3}	4_{g3}	6	8	7	8
9	7	9	11	4_{g3}	6	11	14
8	6_{g4}	6	5	7	6	8	9

Figure 16. Image of total cost, S(i, j): after the first pass (top to bottom)

can be decided experimentally during the road detection part discussed in the earlier section.

Since the three attributes of a line pixel are equally important they should have equal parts in the cost evaluation. However, since they are hardly sensed equally by an actual program, it is proper that their effects on the cost evaluation be proportional to their sensitivities and accuracies. For example, in our detection procedure, the angle of a line pixel is not so accurate as the other attributes. Their proportion in our case turned out to be well described by the following equation,

$$S : B : D = 10 : 2 : 5 \qquad (5.3.33)$$

7	9	9	3	0_{s1}	2	1	0_{s2}
8	5	4	5	2	0_{s1}	1	7
6	7	7	4	1	6	7	6
8	9	6	8	3	6	10	10
7	5*	5	4	5	4	6	7
8	5	4_{g3}	4_{g3}	6	8	7	8
9	7	9	11	4_{g3}	6	11	14
8	6_{g4}	6	5	7	6	8	9

Figure 17. Image of total cost, S(i, j): after the second pass (bottom to top)

In other words, when the others are fixed, the variation of the angle affects the cost at the magnitude of 1 to 2. Similarly the strength and the gray-tone distance solely affect the cost at the magnitude of 1 to 10 and 1 to 5, respectively. Based on the above strategies, the cost of a road pixel is set to zero and the cost of a non-line pixel to 1000. The cost for a non-road line pixel (i, j) is given by

$$C(i, j) = \frac{g(B_{ij})\ h(D_{ij})}{f(S_{ij})} \qquad (5.3.34)$$

The functions g, h, f in Eq. (3.3.34) are defined as follows.

7	9	9	3	0_{s1}	2	1	0_{s2}
8	5	4	5	2	0_{s1}	1	7
6	7	7	4	[1]	6	7	6
8	9	6	8	[3]	6	10	10
7	5	5	[4]	5	4	6	7
8	5	4_{g3}	4_{g3}	6	8	7	8
9	7	9	11	4_{g3}	6	11	14
8	6_{g4}	6	5	7	6	8	9

Figure 18. Image of total cost, S(i, j): after the third pass (top to bottom)

$$g(B) = \begin{cases} 5 & B < LB \\ \dfrac{5*B}{UB - LB} & LB \le B \le UB \\ 10 & B > UB \end{cases} \qquad (5.3.35)$$

where LB and UB are lower and upper limits of angle difference (see figure 20).

$$h(D) = \begin{cases} 2 & D < LD \\ \dfrac{8*D}{UD - LD} & LD \le D \le UD \\ 10 & D > UD \end{cases} \qquad (5.3.36)$$

where LD and UD are lower and upper limits of gray-tone distance (see figure 21).

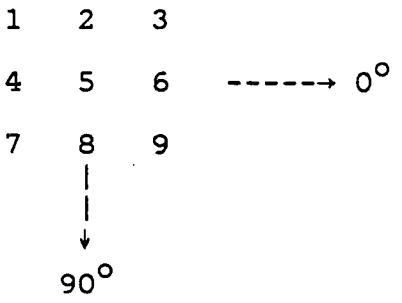

Figure 19. The angle direction

$$f(S) = \begin{cases} 1 & S < LS \\ \dfrac{9*S}{US - LS} & LS \le S \le US \\ 10 & S > US \end{cases} \qquad (5.3.37)$$

where LS and US are lower and upper limits of line strenth (see figure 22).

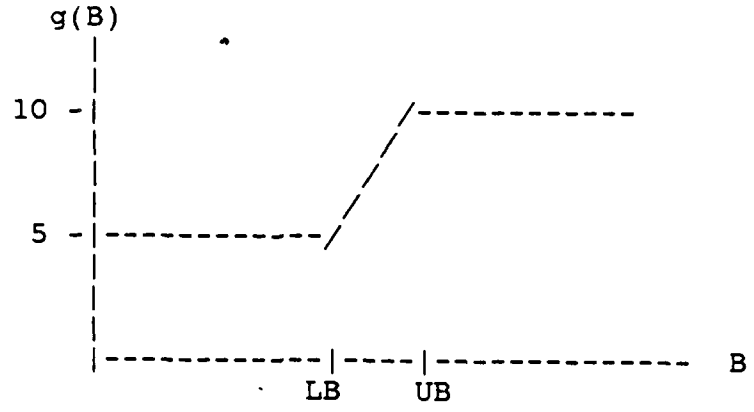

Figure 20. The angle difference function

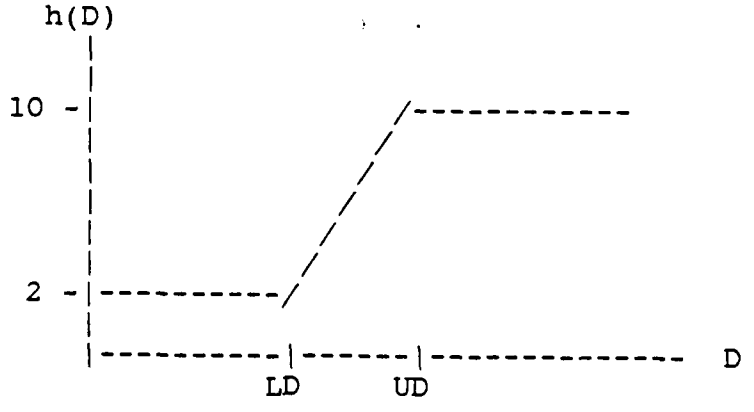

Figure 21. The gray-tone distance function

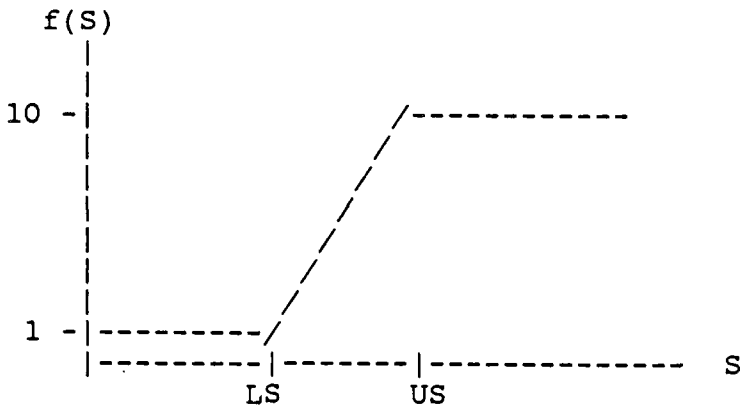

Figure 22. The strength function

CHAPTER 4 FINAL RESULTS

A few SAR images were used as test images. Most of our experiments were carried out on 100 x 100-pixel subimages of them. Figures 23 through 26 show an original subimage and its intermediate and final results. Figures 27 through 30 show a 512 x 512-pixel image and its intermediate and final results.

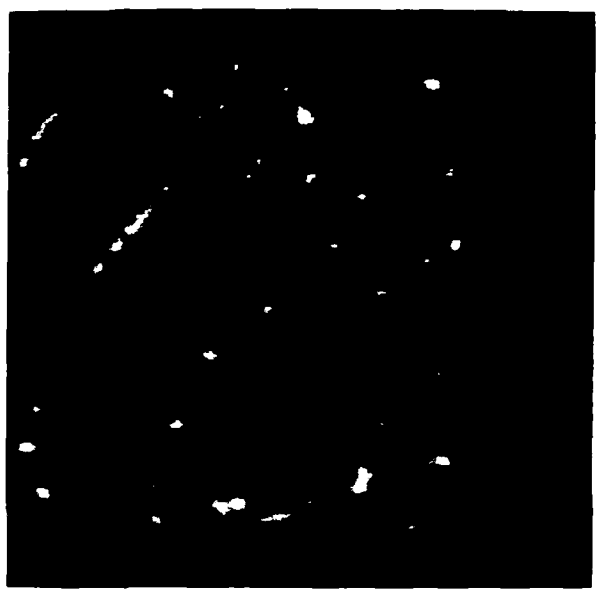

Figure 23. Subimage-1: 100 x 100-pixel image

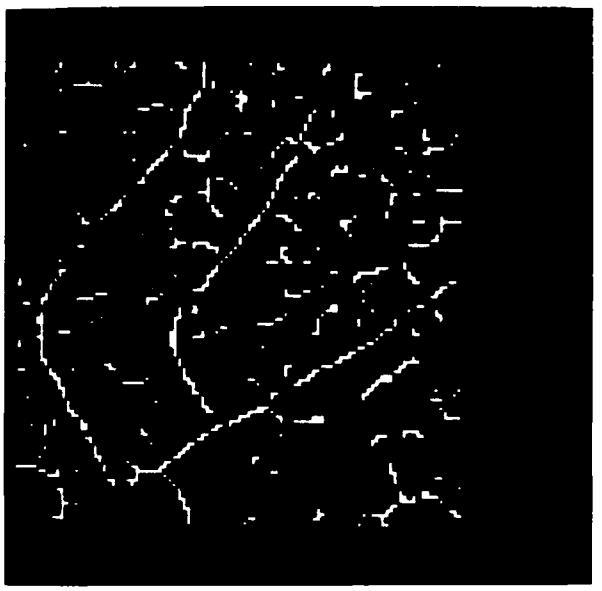

Figure 24. Line image: Radius = 1.0, Curvature = 750, Equiv. range = 1800 -- 2700 Width = 1 -- 4, Contrast = 100

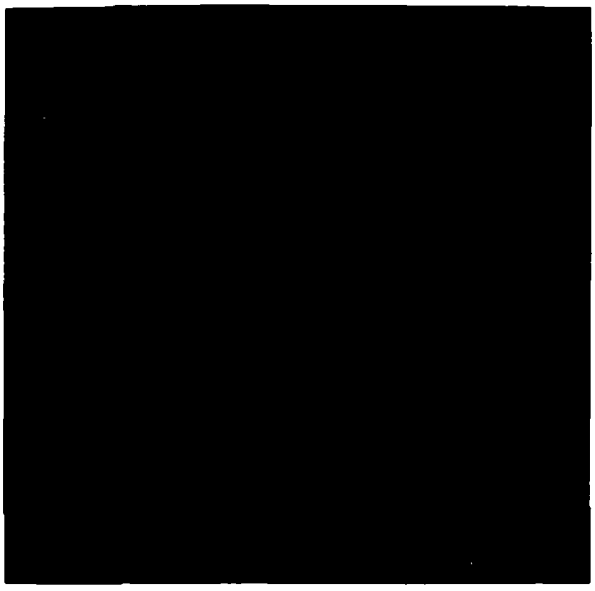

Figure 25. Screened road image: N = 15, MS = 1200, MB = 20, MG = 25,000

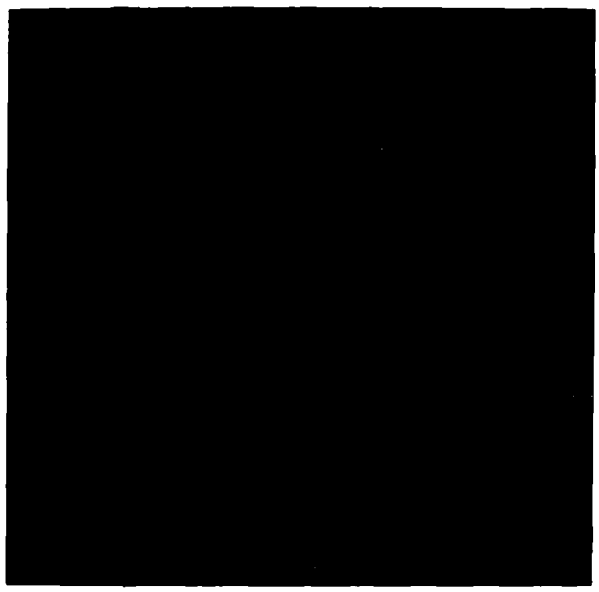

Figure 26. Reconstructed Network image

Figure 27. Elizabeth City area: 512 x 512-pixel image

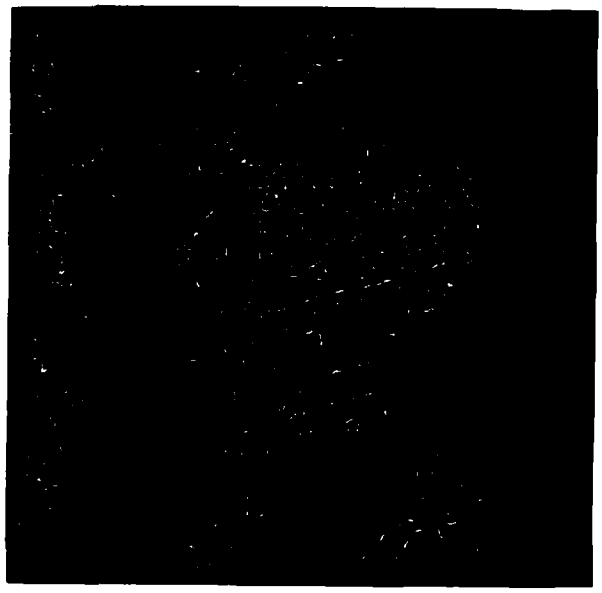

Figure 28. Line image: Radius = 1.3, Curvature = 750, Window size = 9 x 9, Equi. range = 1800 -- 2700, Width = 1 -- 4, Contrast = 50

Figure 29. Screened road image: N = 16, MS = 1250, MB = 15, MG = 25,000

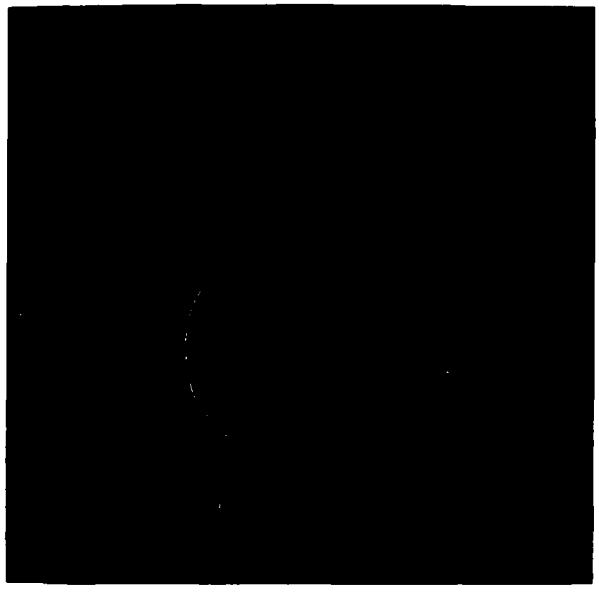

Figure 30. Reconstructed road network image: There are still missing roads and falsely connected roads.

CHAPTER 5 RELATED WORK

There are not many published papers closely related to our work. Here we summarize a few papers related to the road detection on an image. In general, a road network detection involves road segment detection and road connection techniques.

Fischler et al. [5] integrated several road segment techniques. Those operators used are classified either into the type I operator that will hardly mistake artifacts as road segments but often miss true instances, or into the type II operator that will measure parameters of all true instances but may falsely classify and parameterize non-instances. The combined results of a set of type I operators produce the skeleton of a road network, which is then completed by an optimization algorithm, on the basis of a cost array evaluated by the results of type I and type II operators.

Bajcsy and Tavakoli [9] start with the strip detector which finds the connected road pixels (strip) by thresholding gray-tone values. The strips are further thresholded by their contrasts with adjacent regions, and the widths and lengths of themselves. A road segment (piece) consists of two or more connected strips. Then road segments are con-

nected by the directional proximity and distance proximity which look for the minimal angle difference and minimal distance between adjacent disconnected road segments.

VanderBrug [10] detects road segments in satellite imagery without further connection processes during his experiments of semilinear line detector as a compromise between linear and non-linear line detectors.

Most of road segment detection techniques including all of the algorithms mentioned above are based on discrete line or edge detectors that have to use many directional and discrete masks to obtain a pixel information. However, since our road segment scheme used in this report is based on a facet model, the required information is computed analytically. This is the main difference between our technique and others.

CHAPTER 6 CONCLUSIONS AND SUGGESTIONS FOR FURTHER WORK

We began this report with the analysis of road characteristics appearing in radar imagery by understanding a radar system and proceeded to build a road network detection procedure.

In chapter 2, we found that the kernel of a facet model could be viewed as the functon which can be used to compute a facet model according to its arguments such as basis function, the order of fit, index set, and an input digital image. Using this fuction, we obtained a bicubic facet model. It was then found that linear features were analytically detected on the basis of the bicubic facet model. This analytical detection technique made it possible that on a given image, most of the linear features were easily detected and parameterized for their possible attributes such as line orientations, strengths, and widths.

We then faced, in chapter 3, the problem of screening the detected linear features on a pixel by pixel base. The altanative was screening them on a component by component base. This method used the statistics of each maximally connected set of pixels, called a component, and the road characteristics appearing in radar imagery. Using this

method, we were able to obtain a relatively small number of real road segments. We then saw, in section 3.3, that these road segments were connected by the dynamic programming algorithm. This algorithm, based on the "principle of optimality", gave a minmum cost path between two sets of road segments. The costs used in this algorithm were evaluated by the cost evaluation function which measured a merit for each pixel. The dynamic programming algorithm was applied iteratively as many times as the number of the paths required to connect all the road segments.

There are a few directions in which the work in this report could be continued. The most obvious is the method of applying the connection procedure. The method used in this report was to apply the procedure to the whole image. This required a relatively long processing time and hence it had to reduce the mumber of road segments to connect as possible as it could. Since we know the locations of the starting road segments, if the locations of the goal road segments could be correctly guessed with the global context, we could greatly reduce the search area and the processing time.

The cost evaluation function described in section 4.3 could be made to reflect the real situation so that the connection procedure would never mistakenly connect the road segments with non-existent paths.

Another possible improvement would be the fitting surface. The surface used in this report was the bicubic polynomial, which was too general for our line dection purpose. By using a biquadratic or a constrained form of a bicubic polynomial, we may reduce the computatinal complexity. For instance, if the fitted surface was of the form,

$$f(r,c) = A\,(r\cos\alpha + c\sin\alpha)^3 + B\,(r\cos\alpha + c\sin\alpha)2 + C\,(r\cos\alpha + c\sin\alpha) + D \qquad (8.0.38)$$

we would directly obtain the cross-section of the surface simply by replacing $(r\cos\alpha + c\sin\alpha)$ with ρ, where α would be the direction normal to an assumed line as discussed in the section 2.3. It may require deeper mathematical insight as well as laborious research to find proper basis functions but the considerably faster computation would be worth it.

REFERENCES

1. F. F. Sabins, Jr., Remote sensing, W. H. Freeman and Co., San Francisco, 1978

2. R. M. Haralick, "Ridges and valleys on digital images," CVGIP 21, 1983, pp 28-38

3. R. M. Haralick and L. Watson, "A facet model for image data," CGIP 15, 1981, pp 113-129

4. R. M. Haralick, "Digital step edges from zero crossing of second directional derivatives," IEEE Trans. PAMI PAMI-6, NO. 1, 1984, pp 58- 68

5. M. A. Fischler, J. M. Tenenbaum, and H. C. Wolf, "Detection of roads and linear structure in low-resolution aerial imagery using a multisource knowledge integration technique," CGIP 15, 1981, pp 201-223

6. T. C. Hu, Combinatorial Algorithms, Addison-Wesley, 1982

7. L. R. Ford, Jr., Network Flow Theory, The RAND Corp., P-923, 1956

8. R. O. Duda and P. E. Hart, Pattern Classification and Scene Analysis, Wiley, New York, 1973

9. R. Bajcsy and M. Tavakoli, "Computer recognition of road from satellite pictures," IEEE Trans. Syst., Man, Cybern. SMC-16, No. 9, 1976, pp 623-637 pp 37-44

10. G. J. VanderBrug, "Line detection in Satellite imagery," IEEE Trans. Geosci. Electron. GE-14, No. 1, 1976,

DTIC

END

4-86